Electronic Supplementary Material (ESI) for New Journal of Chemistry.
This journal is © The Royal Society of Chemistry and the Centre National de la Recherche Scientifique 2020

Electronic Supplementary Information

Hierarchically interconnected ZnO nanowires for low temperature operated reducing gas sensors: Experimental and DFT studies

Parameshwar R. Chikate,[a] Alfa Sharma,[a] Sachin R. Rondiya,[b] Russell W. Cross,[b] Nelson Y. Dzade,[b] Parasharam M. Shirage,[a] and Rupesh S. Devan[a]*

[a]Department of Metallurgy Engineering & Materials Science, Indian Institute of Technology Indore, Simrol, Indore 453552, India, *E-mail: rupesh@iiti.ac.in

[b]School of Chemistry, Cardiff University, Cardiff, CF10 3AT, Wales, United Kingdom.

A) FESEM Analysis

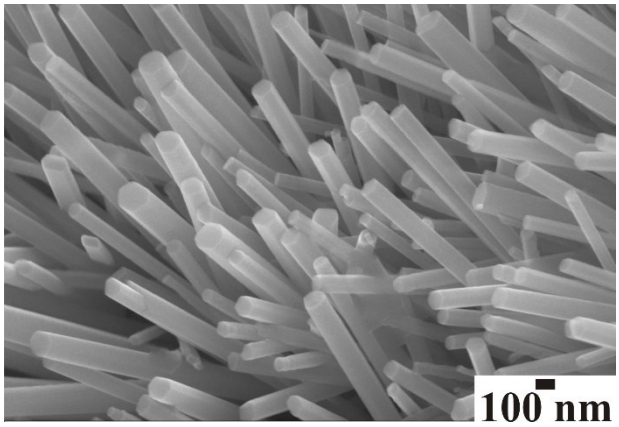

Fig. S1. Higher resolution FESEM image of the portion of large-area arrays of ZnO nanowires.

B) XRD measurements

The phase purity and crystal structure of as-synthesis ZnO nanowires were analyzed from X-ray diffraction (XRD) studies. Fig. 2 shows diffraction peaks located at 31.7^0, 34.4^0, 36.2^0, 47.5^0, 56.5^0, 62.8^0, 66.3^0, 67.9^0, 69.0^0, 72.5^0, and 76.9^0 are well indexed to the (100), (002), (101), (102), (110), (103), (200), (112), (201), (004), and (202) crystalline plane, respectively, of hexagonal wurtzite phase of ZnO (JCPDS Card No. 76-0704) allotted to the space group of *P63mc*

(lattice constants, $a = b = 3.25$ Å and $c = 5.21$ Å). The dominant peaks centered at 31.72^0 and 36.20^0 confirm the preferred growth orientations of the randomly aligned ZnO nanowires along the (100) and (101) directions. The greater thickness of ZnO nanowires has resulted in the untraceable diffraction peaks of the ITO thin film. This confirms the growth of hexagonal wurtzite ZnO nanowires without any defect or impurity phase. Therefore, present hexagonal ZnO nanowires with a high degree of crystallinity are expected to enable better sensing response for hazardous and toxic gases like CO, C_2H_5OH, NH_3, etc.

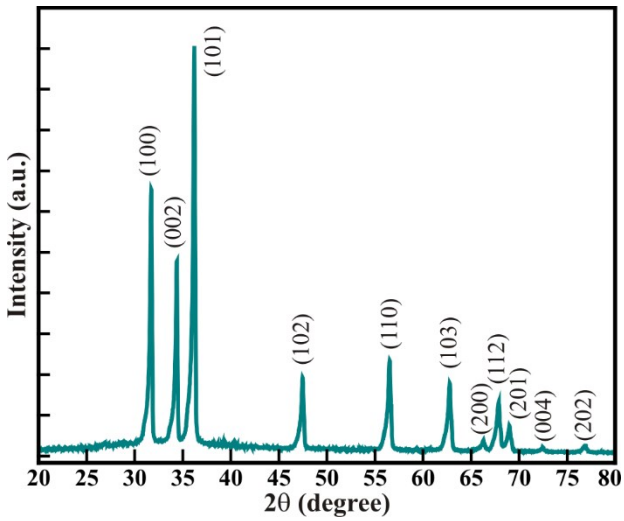

Fig. S2 XRD spectra of large-area arrays of ZnO nanowires.

C) Gas Sensing Measurements

Table S1: The comparative parameters obtained from the Raman scattering spectra of hexagonal ZnO nanowires, and ZnO nanowires (@Si),[1] micro-tubes,[2] quantum dots,[4] and bulk wurtzite structure[4] reported in the literature.

Raman mode / Morphology	A_1	A_1	E_2	A_1	E_1	Reference
ZnO nanowires	328	373	431	530	576	Present work
ZnO Nanowires/Si	332	-	436.5	-	583	[1]
Δf(nanowires-nanowires/Si)	-4		-5.6		-7	
ZnO micro-tubes	331	377	437	-	-	[2]
Δf(nanowires-micro-tubes)	-3	-4	-6			

ZnO quantum dots	348	-	440	-	576	[3]
Δf(nanowires-quantum dots)	-10		-9		0	
Bulk Wurtzite ZnO	333	378	438	536	590	[4]
Δf(nanowires- bulk)	-5	-5	-7	-6	-14	

Table S2: The comparative summary of the response and recovery time of ZnO nanostructure for CO gas.

Morphology	**Response and recovery time (Sec.)**	**Gas concentration**	**Reference**
ZnO nanowires	15.1 and 12.5	50 ppm	Present work
ZnO tetrapods	~ 55 and >100	50 ppm	[5]
ZnO nanowires	20 and 60	500 ppm	[6]
ZnO nanoflowers	25 and 150	200 ppm	[7]
Au adsorbed ZnO nanowires	40 an 80	50 ppm	[8]
ZnO honeycomb structure	~180 and ~210	500 ppm	[9]

Table S3: The comparative summary of the sensing performance of ZnO nanostructure-based CO gas sensors.

Morphology	**Response**	**Temperature (°C)**	**Reference**
ZnO nanowires	31.9 % for 50 ppm	100	Present work
ZnO nanorods	2 % for 50 ppm	350	[10]
flower-like ZnO microstructures	3.8 % for 200 ppm	400	[11]
ZnO tetrapods and nanoparticles	< 20 % for 50 ppm	250	[5]
ZnO nanowires by VLS method	1.5 % for 50 ppm	250	[12]
Co-doped ZnO nanorods	16 % for 50 ppm	350	[10]
Pd-ZnO thin film	7 % for1000 ppm	200	[13]
Pt-ZnO nanosheets	3.57 % for 50 ppm	180	[14]
Al-ZnO nanoparticles	1.6 for 50 ppm	300	[15]

Table S4: The comparative summary of the sensing performance of ZnO nanostructure-based C_2H_5OH gas sensors.

Morphology	Response	Temperature (^oC)	Reference
ZnO nanowires	101.9 % @50 ppm	100	Present work
ZnO nanoplates	23.3 %for 400 ppm	350	[16]
hierarchical ZnO nanoflowers	30.4 % for 400 ppm	350	[16]
sputtered ZnO film	6.2 % for 100 ppm	400	[17]
ZnO nanorods	1.6 % for 50 ppm	350	[10]
flower-like ZnO microstructures	3.5 % for 50 ppm	400	[11]
vertically aligned ZnO nanorods	1.33 % for 500 ppm	260	[18]
Ta doped ZnO thin film	9.8 % for 100 ppm	400	[17]
Co-doped ZnO nanorods	1.85 % for 50 ppm	350	[10]
TiO_2 modified ZnO tetrapods	~ 20 % for 50 ppm	300	[5]
Pd-nanoparticle decorated ZnO nanorods	5.12 % for 500 ppm	260	[18]
high density Pd-ZnO nanowires	44.5 % for 500 ppm	170	[19]
ZnO nanowires	190 % for 200 ppm	500	[20]
NiO/ZnO nanoplates	37.5 % for 500 ppm	400	[21]
Ag/ZnO nanocomposite	~100 % for 500 ppm	400	[22]
CuO/ZnO nanocomposite	~100 % for 500 ppm	400	[23]
Urchin like 1-D ZnO nanorod	180 for 100 ppm	300	[24]

Table S5: The comparative summary of the response and recovery time of ZnO nanostructure for NH_3 gas.

Morphology	Response and recovery time (Sec.)	Gas concentration	Reference
ZnO nanowires	18.3 and 10.8	50 ppm	Present work
defect controlled ZnO nanorods	64 and 28	25 ppm	[25]

tapered ZnO nanostructures	49 and 19	25 ppm	[25]
Cu-doped ZnO	32 and 56	100 ppm	[26]
ZnO nanorods	351 and 125	1000 ppm	[27]
ZnO nanoparticles	660 and 160	600 ppm	[28]
Cd/Mg/Y doped ZnO	183/49 and 162/58	50 ppm	[29]

Table S6: The comparative summary of the sensing performance of ZnO nanostructure-based NH_3 gas sensors.

Morphology	Response	Temperature (^oC)	Reference
ZnO nanowires	115.9 for 50 ppm 128.9 for 100 ppm	100	Present work
Vertical ZnO nanorods	~ 5 % for 100 ppm	150	[25]
Tapered ZnO nanostructures	~ 85 % for 100 ppm	150	[25]
ZnO nanorods	10.1 % for 100 ppm	300	[27]
ZnO nanoflowers	49.5 % for 50 ppm	250	[30]
Fe doped ZnO thick film	75 % for 50 ppm	30	[31]
Al monodoped n-ZnO	< 10 % for 600 ppm	100	[32]
AlN codoped p-ZnO	< 20 % for 600 ppm	100	[32]
AlAs codoped p-ZnO	< 65 % for 600 ppm	100	[32]
Al-doped ZnO nanoflowers	33 % for 75 ppm	190	[33]
Cu-doped ZnO nanoellipsoids	12.9 % for 100 ppm	100	[26]
Mn-doped ZnO microspheres	8.9 % for 100 ppm	100	[34]
Ag-doped ZnO nanoellipsoids	29.5 % for 100 ppm	150	[35]
Al-doped ZnO thin film	40 % for 75 ppm	160	[36]
ZnO- GrO nanocomposite	~24 % for 1 ppm	30	[37]

D) Sensing mechanism for NH_3 gas

The sensing responses of ZnO nanowires has increased up to 100 °C and then decreased with an increase in temperature. The temperature-dependent response of the ZnO nanowires can be ascribed to the operating temperature. Moreover, the literature illustrates that O_2 (oxygen molecules) generally physisorbed on the metal oxide surface at low temperature (>100 °C) and form O_2^- (ads) ions, but at moderate (100-300 °C) and high (< 300 °C) temperature the chemisorption results in to O^- and O^{2-} ions respectively.[35,38,39] Therefore, after exposing ZnO with reducing gas like NH_3 at moderate temperature, the oxygen species interact with NH_3 molecules to release the electrons to the conduction band, which can be given by the reaction

$$4NH_3 + 3O_2^- \rightarrow 6H_2O + 2N_2 + 3e^- \quad \text{-(S2)}$$

These free electrons are given back to the conduction band of ZnO and result to increase in carrier concentration to an extent. This leads to a decrease in electrical resistance of the ZnO nanowires in the ammonia environment. However, the possible reaction at high temperature (> 100 °C) is

$$2NH_3 + 3O^- \rightarrow 3H_2O + N_2 + 3e^- \quad \text{-(S3)}$$

The above redox processes confirm that four NH_3 molecules react with three O_2^- to release 3 electrons (i.e., eq. S1), while at temperature > 100 °C two NH_3 molecules are sufficient to react with O^-. However, the mechanism of interactions becomes more complicated at temperature >100 °C in the ammonia environment due to the presence of many types of adsorbed species on the surface in atomic and molecular forms.[40] There is a possibility of formation of NO_x in the presence of oxygen species as represented below,

$$4NH_3 + 5O_2^- \rightarrow 6H_2O + 4NO + 5e^- \quad \text{-(S4)} \qquad \text{Or}$$

$$2NH_3 + 4O_0 \rightarrow 3H_2O + N_2O + 8e^- \quad \text{-(S5)}$$

$$2NH_3 + 3O_0 \rightarrow 3H_2O + 2NO + 10e^- \quad \text{-(S6)}$$

In such formation of oxidizing NO_x, the thickness of the depletion layer increases, and hence the electrical resistance of metal oxides increases.[32] But, the decrease in the electrical resistance of our samples in the ammonia environment rules out the formation of NO_x and gas sensing mechanisms related to it. Thus, our experimental conditions propose the formation of N_2 only and not NO_x by the reaction on NH_3.

References

[1] C. Y. Geng, Y. Jiang, Y. Yao, X. M. Meng, J. A. Zapien, C. S. Lee, Y. Lifshitz, and S. T. Lee, *Adv. Funct. Mater.,* 2004, **14**, 589-594.

[2] Z. W. Dong, C. F. Zhang, H. Deng, G. J. You, and S. X. Qian, *Mater. Chem. Phys.,* 2006, **99**, 160-163.

[3] A. G. Milekhin, N. A. Yeryukov, L. L. Sveshnikova, T. A. Duda, C. Himcinschi, E. I. Zenkevich, and D. R. T. Zahn, *Appl. Phys. A-Mater. Sci. Process.,* 2012, **107**, 275-278.

[4] R. Cusco, E. Alarcon-Llado, J. Ibanez, L. Artus, J. Jimenez, B. G. Wang, and M. J. Callahan, *Phys. Rev. B,* 2007, **75**, 165202.

[5] T. Santhaveesuk, K. Shimanoe, K. Suematsu, and S. Choopun, *Phys. Status Solidi A-Appl. Mat.,* 2018, **215**, 1700784.

[6] T. J. Hsueh, Y. W. Chen, S. J. Chang, S. F. Wang, C. L. Hsu, Y. R. Lin, T. S. Lin, and I. C. Chen, *Sens. Actuator B-Chem.,* 2007, **125**, 498-503.

[7] T. Krishnakumar, R. Jayaprakash, N. Pinna, N. Donato, A. Bonavita, G. Micali, and G. Neri, *Sens. Actuator B-Chem.,* 2009, **143**, 198-204.

[8] S. J. Chang, T. J. Hsueh, I. C. Chen, and B. R. Huang, *Nanotechnology,* 2008, **19**, 175502.

[9] C. S. Prajapati, D. Visser, S. Anand, and N. Bhat, *Sens. Actuator B-Chem.,* 2017, **252**, 764-772.

[10] Y. J. Li, K. M. Li, C. Y. Wang, C. I. Kuo, and L. J. Chen, *Sens. Actuator B-Chem.,* 2012, **161**, 734-739.

[11] P. Rai, S. Raj, K. J. Ko, K. K. Park, and Y. T. Yu, *Sens. Actuator B-Chem.,* 2013, **178**, 107-112.

[12] J. H. Kim, A. Mirzaei, H. W. Kim, and S. S. Kim, *ACS Appl. Mater. Interfaces,* 2019, **11**, 24172-24183.

[13] W. T. Moon, Y. K. Jun, H. S. Kim, W. S. Kim, and S. H. Hong, *J. Electroceram.,* 2009, **23**, 196-199.

[14] Y. Wang, X. N. Meng, and J. L. Cao, *J. Hazard. Mater.,* 2020, **381**, 120944.

[15] M. Hjiri, L. El Mir, S. G. Leonardi, A. Pistone, L. Mavilia, and G. Neri, *Sens. Actuator B-Chem.,* 2014, **196**, 413-420.

[16] L. Zhu, Y. Q. Li, and W. Zeng, *Appl. Surf. Sci.,* 2018, **427**, 281-287.

[17] X. Huang, C. P. Li, L. R. Qian, M. J. Li, H. J. Li, X. C. Niu, and B. H. Yang, *Mater. Today Commun.,* 2019, **21**, 100680.

[18] P. Cao, Z. Yang, S. T. Navale, S. Han, X. Liu, W. Liu, Y. Lu, F. J. Stadler, and D. Zhu, *Sens. Actuator B-Chem.,* 2019, **298**, 126850.

[19] T. J. Hsueh, S. J. Chang, C. L. Hsu, Y. R. Lin, and I. C. Chen, *Appl. Phys. Lett.,* 2007, **91**, 053111.

[20] D. Zappa, E. Comini, and G. Sberveglieri*, Nanotechnology, 2013, **24**, 444008.*

[21] X. Deng, L. Zhang, J. Guo, Q. Chen, and J. Ma*, Mater. Res. Bull., 2017, **90**, 170-174.*

[22] Q. Simon, D. Barreca, A. Gasparotto, C. Maccato, E. Tondello, C. Sada, E. Comini, A. Devi, and R. A. Fischer*, Nanotechnology, 2012, **23**, 025502.*

[23] Q. Simon, D. Barreca, A. Gasparotto, C. Maccato, E. Tondello, C. Sada, E. Comini, G. Sberveglieri, M. Banerjee, K. Xu, A. Devi, and R. A. Fischer, *ChemPhysChem, 2012, **13**,2342-2348.*

[24] D. Barreca, D. Bekermann, E. Comini, A. Devi, R. A. Fischer, A. Gasparotto, C. Maccato, C. Sada, G. Sberveglieri, and E. Tondello, *CrystEngComm, 2012, **12**, 3419-3421.*

[25] P. S. Venkatesh, P. Dharmaraj, V. Purushothaman, V. Ramakrishnan, and K. Jeganathan, *Sens. Actuator B-Chem.,* 2015, **212**, 10-17.

[26] R. S. Ganesh, E. Durgadevi, M. Navaneethan, V. L. Patil, S. Ponnusamy, C. Muthamizhchelvan, S. Kawasaki, P. S. Patil, and Y. Hayakawa, *Sens. Actuator A-Phys.,* 2018, **269**, 331-341.

[27] T. Y. Chen, H. I. Chen, C. S. Hsu, C. C. Huang, J. S. Wu, P. C. Chou, and W. C. Liu, *Sens. Actuator B-Chem.,* 2015, **221**, 491-498.

[28] C. F. Li, C. Y. Hsu, and Y. Y. Li, *J. Alloy. Compd.,* 2014, **606**, 27-31.

[29] E. Vinoth, and N. Gopalakrishnan, *J. Alloy. Compd.,* 2020, **824**, 153900.

[30] Y. Zhang, T. M. Liu, J. H. Hao, L. Y. Lin, W. Zeng, X. H. Peng, and Z. C. Wang, *Appl. Surf. Sci.,* 2015, **357**, 31-36.

[31] G. S. T. Rao, and D. T. Rao, *Sens. Actuator B-Chem.,* 1999, **55**, 166-169.

[32] L. N. Balakrishnan, S. Gowrishankar, and N. Gopalakrishnan, *IEEE Sens. J.,* 2013, **13**, 2055-2060.

[33] F. Ozutok, I. Karaduman, S. Demiri, and S. Acar, *J. Electron. Mater.,* 2018, **47**, 2648-2657.

[34] R. S. Ganesh, E. Durgadevi, M. Navaneethan, V. L. Patil, S. Ponnusamy, C. Muthamizhchelvan, S. Kawasaki, and P. S. Patil, Hayakawa, *J. Alloy. Compd.,* 2017, **721**, 182-190.

[35] R. S. Ganesh, M. Navaneethan, V. L. Patil, S. Ponnusamy, C. Muthamizhchelvan, S. Kawasaki, P. S. Patil, and Y. Hayakawa, *Sens. Actuator B-Chem.,* 2018, **255**, 672-683.

[36] Y. Hou, A. M. Soleimanpour, and A. H. Jayatissa*, Sens. Actuator B-Chem.,* 2013, **177**, 761-769.

[37] G. Singh, A. Choudhary, D. Haranath, A. G. Joshi, N. Singh, S. Singh, and R. Pasricha, Carbon, 2012, **50**, 385-394.

[38] A. Sharma, P. Bhojane, A. K. Rana, Y. Kumar, and P. M. Shirage, *Scr. Mater.,* 2017, **128**, 65.

[39] I. Rawal, *RSC Adv.,* 2015, **5**, 4135-4142.

[40] K. K. Khun, A. Mahajan, and R. K. Bedi, *J. Appl. Phys.,* 2009, **106**, *124509.*